Journal of Electroceramics 3:1, 37–46, 1999


# Properties of Pyrochlore Ruthenate Cathodes for Intermediate Temperature Solid Oxide Fuel Cells

J.-M. BAE & B. C. H. STEELE
*Dept. of Materials, Imperial College, London, UK*

Submitted March 13, 1998; Revised October 16, 1998; Accepted October 21, 1998

**Abstract.** Powders of $Bi_2Ru_2O_{7.3}$, $Pb_2Ru_2O_{6.5}$, and $Y_2Ru_2O_7$ were prepared and their reactivity with $Ce_{0.9}Gd_{0.1}O_{1.95}$ (CGO) electrolyte powders examined. $Bi_2Ru_2O_{7.3}$ and $Pb_2Ru_2O_{6.5}$ reacted with CGO but $Y_2Ru_2O_7$ appeared stable when heated in contact with CGO powder at 900C for 24 h. Symmetrical electrodes of $Y_2Ru_2O_{7-x}$ were deposited on CGO ceramic pellets, either by tape-casting or by electrostatic assisted chemical vapor deposition (EACVD) techniques, and cathode resistivities determined by impedance spectroscopy. Undoped $Y_2Ru_2O_7$ electrodes exhibited very high area specific resistivities (ASR) at 627C ( $\sim 4000\,\Omega cm^2$), but by doping with SrO the resistivity was reduced almost $100\times$ to $47\,\Omega cm^2$. The behavior of the $Y_2Ru_2O_7$ cathodes was interpreted in terms of available oxygen ion transport data for the $Gd_2Ti_2O_7$ series, and it was concluded that optimization of pyrochlore ruthenate compositions should be possible to improve further the oxygen reduction behavior of ruthenate cathodes for intermediate temperature solid oxide fuel cells.

**Keywords:** ruthenate pyrochlores, oxide cathodes, IT-SOFC

## 1. Introduction

Noble metal and noble metal oxide powders (e.g., Pt, PdO, $RuO_2$) dispersed on oxide cathodes such as $La_{0.8}Sr_{0.2}MnO_3$ (LSM), $La_{0.6}Sr_{0.4}Co_{0.2}Fe_{0.8}O_3$ (LSCF) have been shown [1–4] to have a beneficial effect in reducing the cathode resistivity in solid oxide fuel cells (SOFC). It is appropriate, therefore, to examine whether noble metal oxides incorporated into oxide solid solutions, including typical oxide cathodes such as LSM and LSCF, can also improve the kinetics of oxygen reduction. Incorporating the noble metal into an oxide structure should reduce the tendency to agglomeration which is a feature of small dispersed particles of noble metals and their oxides. $RuO_2$ was selected as the noble metal oxide as it is stable over the range of temperatures and oxygen partial pressures likely to be encountered in the operation of intermediate temperature (500–700C) solid oxide fuel cells (IT-SOFC). The pyrochlore structure was selected for the present investigation as pyrochlore ruthenates ($A_2^{3+}Ru_2^{4+}O_7$) can exhibit useful electronic conductivities [5], and had already been shown [6–8] to be promising electrocatalysts for oxygen reduction in ambient temperature aqueous electrolyte fuel cells. In the context of IT-SOFC technology the level of oxygen ion conductivity in oxide pyrochlores can also be manipulated [9] either by influencing the energetics of the oxygen vacancy order-disorder process, and/or by the introduction of aliovalent cations. Moreover Tuller et al. [10–12] had provided some preliminary electronic and ionic transport data for compositions in the series: $Gd_2(Ti_{1-x}Ru_x)_2O_7$ for $x$ values up to 0.2. This initial study is therefore concerned with the examination of the following $RuO_2$ containing pyrochlore compositions; $Bi_2Ru_2O_7$, $Pb_2Ru_2O_7$, and $Y_2Ru_2O_7$. In addition $Y_2Ru_2O_7$ was also doped with SrO in an effort to improve the partial oxygen ion conductivity.

## 2. Experimental

### *2.1. Preparation of $Ce_{0.9}Gd_{0.1}O_{1.95}$ (CGO) Electrolyte*

$Ce_{0.9}Gd_{0.1}O_{1.95}$ powder from Seattle Speciality Ceramics was used for fabrication of the electrolytes. The powder was uniaxially pressed at 15 MPa pressure and subsequently isostatically pressed at 300 MPa to ensure a high green body density. Sintering was carried out at 1550C for 5 h.

### *2.2. Ruthenate Powder Preparations*

Lead ruthenate and yttrium ruthenate were prepared by solid state reaction methods. $Pb(NO_3)_2$ from Johnson Matthey Co., and $RuO_2$ from Aldrich Co., were used as the starting materials for lead ruthenate preparation. The two powders were weighed and the mixture placed in a plastic bottle which was rotated for 5 h. The powder was then uniaxially pressed to make a pellet, which was calcined at 850C for 10 h. The pellet was ground and pressed again to make a pellet and calcined for another 10 h at the same temperature. After each calcination, the pellet was ground using an agate pestle and mortar. The excess lead oxide was leached out by nitric acid solution at room temperature. After washing the powders with de-ionized water several times, they were dried at 250C for 10 h.

$Y_2O_3$ and $RuO_2$ powders from Aldrich Co. were used to make yttrium ruthenate. After weighing and mixing, the mixture was uniaxially pressed to make pellets. The pellets were placed in a quartz tube which was filled with 0.5 atm of oxygen gas and then sealed. The quartz tube was next heated at 1150C for 24 h. Any excess of yttrium oxide was removed by the same method as that of lead ruthenate.

A co-precipitation method was used to prepare the bismuth ruthenate powder using $Bi(NO_3)_3 - 5H_2O$ and $RuCl_3$ (Aldrich Co.) as starting materials. 1.5:1 of Bi:Ru cationic ratio was used. The bismuth nitrate was dissolved in 50 vol% nitric acid and the ruthenium chloride in de-ionized water. The two solutions were mixed and diluted to 0.1 mole/l cationic concentration with de-ionized water. The solution was dripped slowly into ammonium hydroxide solution. The precipitate was separated by centrifuge and washed several times in de-ionized water. The hydroxides were calcined at 550C for 10 h to attain bismuth ruthenium oxide. The excess bismuth oxide in the final product was leached out with the same method as that of lead ruthenate.

Strontium-doped yttrium ruthenate was prepared by the citrate route. $Sr(NO_3)_2$ and $Y(NO_3)_3.5H_2O$ (Aldrich Co.) together with $Ru(NO)(NO_3)_3$ (Johnson Matthey Co.) were used as the starting materials. Appropriate amounts of the starting materials were weighed to achieve the required cationic ratios. An amount of citric acid (Aldrich) with molar equivalence to the whole amount of the cations was added to the mixture. The mixture was dissolved in de-ionized water and the solution heated with stirring to evaporate water. When precipitates appeared, several drops of ammonia solution were added to the solution until the precipitates disappeared. When the solution became viscous after most of the water was evaporated, the temperature of the hot plate was increased to about 300–350C. From the viscous solution a foam was obtained and the foam was then combusted. The product was calcined at several temperatures to obtain crystalline ruthenate pyrochlore oxide without organic substances [13,14].

### *2.3. Fabrication of Cathodes*

*2.3.1. Porous thick structures.* A relatively thick and porous ruthenate layer on top of the CGO electrolyte was fabricated by brushing on the relevant ruthenate slurry. The tape-casting slurries were prepared by initially ball-milling the following mixture for 24 h; 120 g of the ceramic powder, 2 g of fish oil, and 72 g of ethanol. Additions of polyvinyl butanol (18 g), polyethylene glycol (4.5 g), dibutyl pthalate (4.5 g), were then made and the slurry ball-milled for a further 24 h. After deposition, the cathode layer was dried by a halogen lamp. The dried sample was finally sintered at 800–900C for 4 h.

*2.3.2. Thick film cathode structures using electrostatic assisted CVD (EACVD).* The EACVD technique was used to fabricate thick film (3–5 $\mu$m) electrodes of $(Y, Sr)_2Ru_2O_7$ on CGO electrolytes. A schematic diagram of the EACVD method is shown in Fig. 1. This process was developed at Imperial College [15] for the fabrication of oxide films and further details, together with subsequent improvement, are available in the literature [16]. An advantage of this fabrication route is that it can be used in normal atmosphere without special environ-

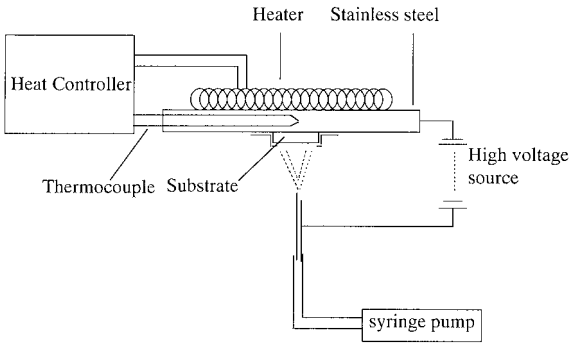


*Fig. 1.* Schematic diagram of electrostatic spray pyrolysis (EACVD) equipment for oxide film fabrication.

mental control. Ruthenium nitrosyl nitrate (Johnson Matthey), yttrium nitrate pentahydrate (Aldrich), strontium nitrate (Aldrich), and cobalt nitrate hexahydrate (Aldrich) were used as the source materials for the ruthenate films. Appropriate amounts of nitrates were dissolved in absolute ethanol with 10–20 vol% of de-ionized water to produce a 0.5–2 cationic mole/litre concentration. The solution was thoroughly mixed using a magnetic stirrer and the liquid supplied to a nozzle at a flow rate of 6–7 ml/h. A high voltage (10–15 KV) was applied between a nozzle and stainless steel hot plate to generate an aerosol of liquid droplets. Using a glass substrate, Zomeren et al. [17] reported that it was necessary to introduce sputtered Pt coatings to prevent charge accumulation during deposition of oxide films by EACVD. However in the present investigation films of $(Y, Sr)_2Ru_2O_7$ were successfully fabricated without the introduction of additional conductive layers provided the film thickness did not exceed 5 $\mu$m. Films were deposited on both sides of $Ce_{0.9}Gd_{0.1}O_{1.95}$ substrates attached to the stainless steel hot plate which was maintained at 300–400C. The films were subsequently heated at 800C for 4 h to produce crystalline ruthenates.

### 2.4. *Electrode Resistivity Measurements*

Impedance spectroscopy was used to measure the electrode resistivity of symmetrical ruthenate electrodes on CGO electrolytes using a computer-controlled Solatron SI 1260 Impedance/Gain-Phase Analyzer with a 50 mV signal The sample was mechanically contacted with spring loaded platinum gauze.

## 3. Results and Discussions

### 3.1. *X-ray Characterization of $Bi_2Ru_2O_{7.3}$ and $Pb_2Ru_2O_{6.5}$ Powders*

Formation of the cubic phases, bismuth ruthenate $(Bi_2Ru_2O_{7.3})$ and lead ruthenate $(Pb_2Ru_2O_{6.5})$, was confirmed by powder X-ray diffraction. The stoichiometries quoted for these compounds are the values reported in the relevant JPCDS files.

To check the reactivity of each ruthenate with CGO, mixtures of the two powders were thoroughly mixed and subsequently uniaxially pressed. The resulting pellets were heated at 800–900C for 24 h. X-ray examination of the bismuth ruthenate/CGO and lead ruthenate/CGO mixtures revealed unidentified extra peaks (Figs. 2 and 3) having a relatively strong intensity. It is therefore probable that the lead ruthenate and bismuth ruthenate electrodes will degrade in contact with CGO electrolytes during long term operation at high temperature. Due to these unidentified reactions, further investigations of lead ruthenate and bismuth ruthenate were not carried out.

It is interesting to note that Linquette-Mailley et al. [18] have recently reported an investigation concerned with the behavior of $Bi_2Ru_2O_{7.3}$ cathodes on stabilized zirconia electrolytes. Although these electrodes were prepared by heating ceramic slurries at 927C the authors do not comment about any evidence, positive or negative, regarding reactions between the electrodes and zirconia electrolyte.

### 3.2. *X-ray and Microstructural Characterization of Yttrium Ruthenate (YRO)*

*3.2.1. Reactivity of $Y_2Ru_2O_7$ powders.* The formation of yttrium ruthenate $(Y_2Ru_2O_7)$ was confirmed by X-ray powder diffraction analysis and the lattice parameter values (10.143 Å) were in good agreement (10.140 Å) with those listed in JPCDS. Pellets of YRO/CGO annealed at 900C for 24 h did not lead to the development of additional peaks (Fig. 4), and lack of reactivity was also confirmed by SEM micrographs (Figs. 5 and 7) of cathode/electrolyte interfaces.

*3.2.2. Thick porous $Y_2Ru_2O_7$ cathodes (15 $\mu$m).* An SEM micrograph (Fig. 5) of a fractured surface of a $Y_2Ru_2O_7/CGO/Y_2Ru_2O_7$ symmetrical sample indicates that the thickness of the electrode is

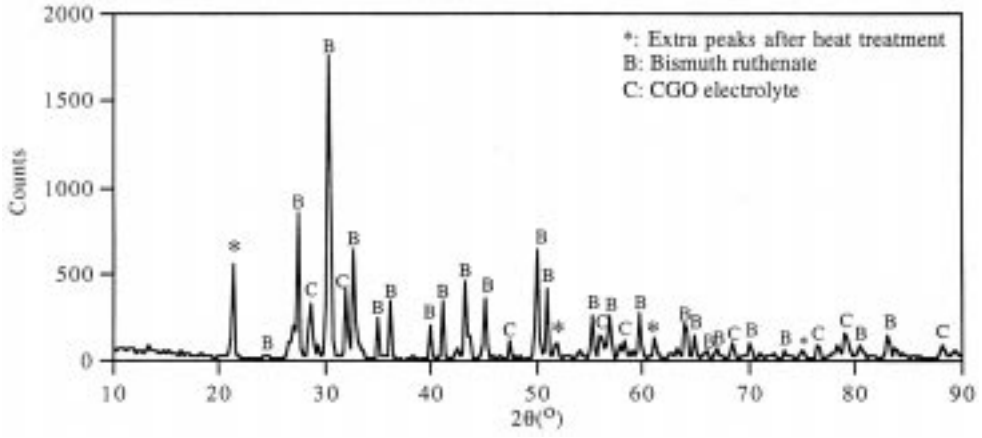


*Fig. 2.* XRD peaks of bismuth ruthenate/CG010 mixture after heat treatment at 800C for 30 h. Extra peaks appeared.

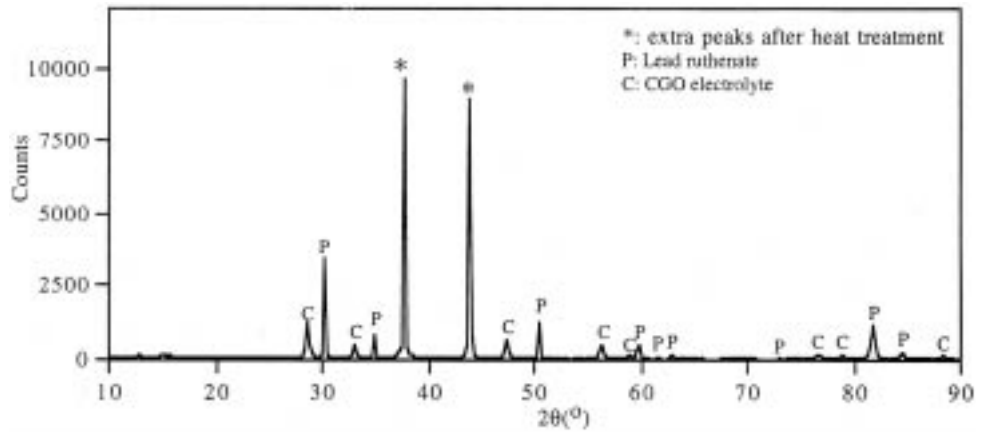


*Fig. 3.* XRD peaks of lead ruthenate/CG010 mixture after heat treatment at 880C for 30 h. Extra peaks appeared.

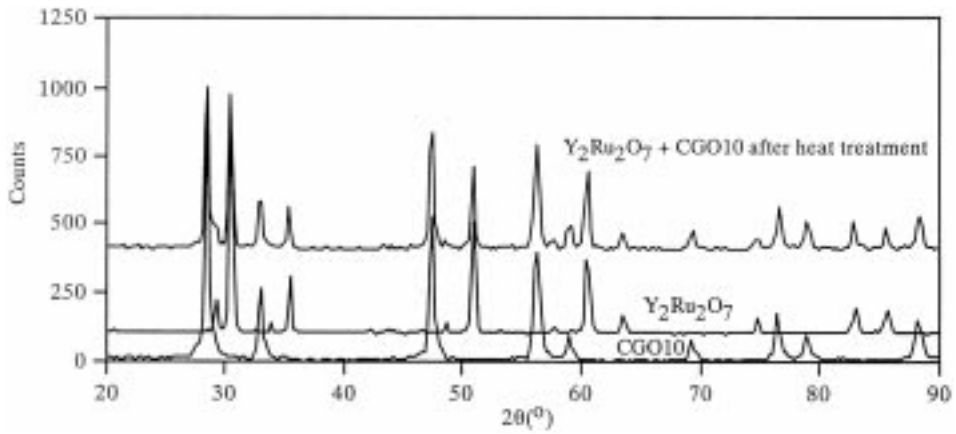


*Fig. 4.* XRD peaks of yttrium ruthenate/CG010 mixture after heat treatment at 900C for 30 h. No extra peaks are exhibited.

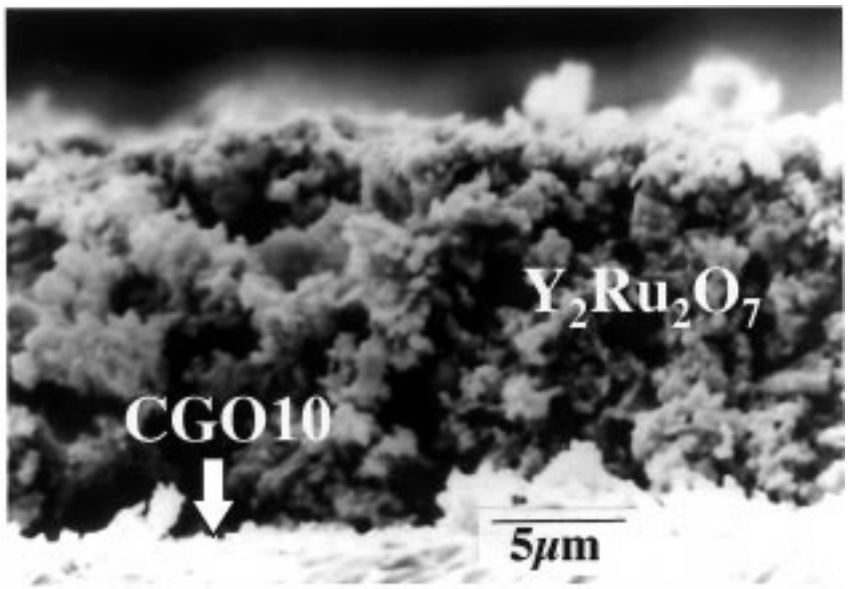


*Fig. 5.* SEM micrograph of fractured surface on yttrium ruthenate/CG010 symmetric sample.

about 15 $\mu$m and the grain size of the electrode is of the order of one micron. As well as examining electrodes fabricated from undoped YRO, the composition $(Y_{0.8}Sr_{0.2})_2Ru_2O_7$ was also prepared by the citrate route, and provided the powders were sintered above 800C in pure oxygen X-ray powder diffraction indicated a single phase pyrochlore structure with the following lattice parameters: 10.163 Å.

*3.2.3. Thin $Y_2Ru_2O_7$ cathodes (3 $\mu$m).* Several compositions of $(Y_{1-x}Sr_x)_2Ru_2O_7$ (YSRO) film electrodes were prepared using the EACVD fabrication route. Good crystalline films of YSRO were obtained (Fig. 6) after the deposited film was annealed at 800C for 4 h, and it appeard that the pyrochlore composition was still retained upto 40 mole% SrO according to X-ray diffraction patterns. The lattice parameters of the composition $(Y_{0.8}Sr_{0.2})_2Ru_2O_7$, for example, had somewhat higher lattice parameters (10.213 Å) compared to those measured (10.163 Å) for the powders of a nominally similar composition prepared by the citrate route. This suggested that the different fabrication routes did not produce cathodes with identical SrO dopant levels, but this dicrepancy was not resolved in the present investigation. It should also be noted that Senzaki et al. [19] have used spray pyrolysis techniques to prepare successfully metal ruthenate powders.

The SEM micrograph of a typical fracture surface (Fig. 7) indicates a fairly dense film of thickness around 3 $\mu$m.

### *3.3. Impedance Measurements*

*3.3.1. Thick porous $Y_2Ru_2O_7$ cathodes (15 $\mu$m).* A typical impedance spectra measured at 623C for an undoped YRO cathode is reproduced in Fig. 8a. The electrode area specific resistivity (ASR) is 4200 $\Omega$cm$^2$, and appears as an offset from zero ($x$-axis) as the total electrolyte resistivity (grain plus grain boundary) is not resolved above 500C. A similar measurement (Fig. 8b) on the doped composition, $(Y_{0.8}Sr_{0.2})_2Ru_2O_7$, indicated a cathode resistivity of 154 $\Omega$cm$^2$ at a comparable temperature, 626C.

The high resistivity of the undoped material suggests that it is behaving in a similar manner to $La_{0.85}Sr_{0.15}MnO_3$ (LSM) at low overpotentials which also exhibits many similarities to porous Pt cathodes [e.g., 20]. The overall oxygen reduction process is believed to involve the dissociative-adsorption of oxygen molecules with rapid electron transfer to form $O^-$, $O^{2-}$, species, which then diffuse over the internal surface of the cathode towards the triple-phase-boundary (tpb). Unless the diffusion path is long, Steele [21] has suggested that the oxygen surface diffusion exchange coefficient (k cm.s$^{-1}$) can be used

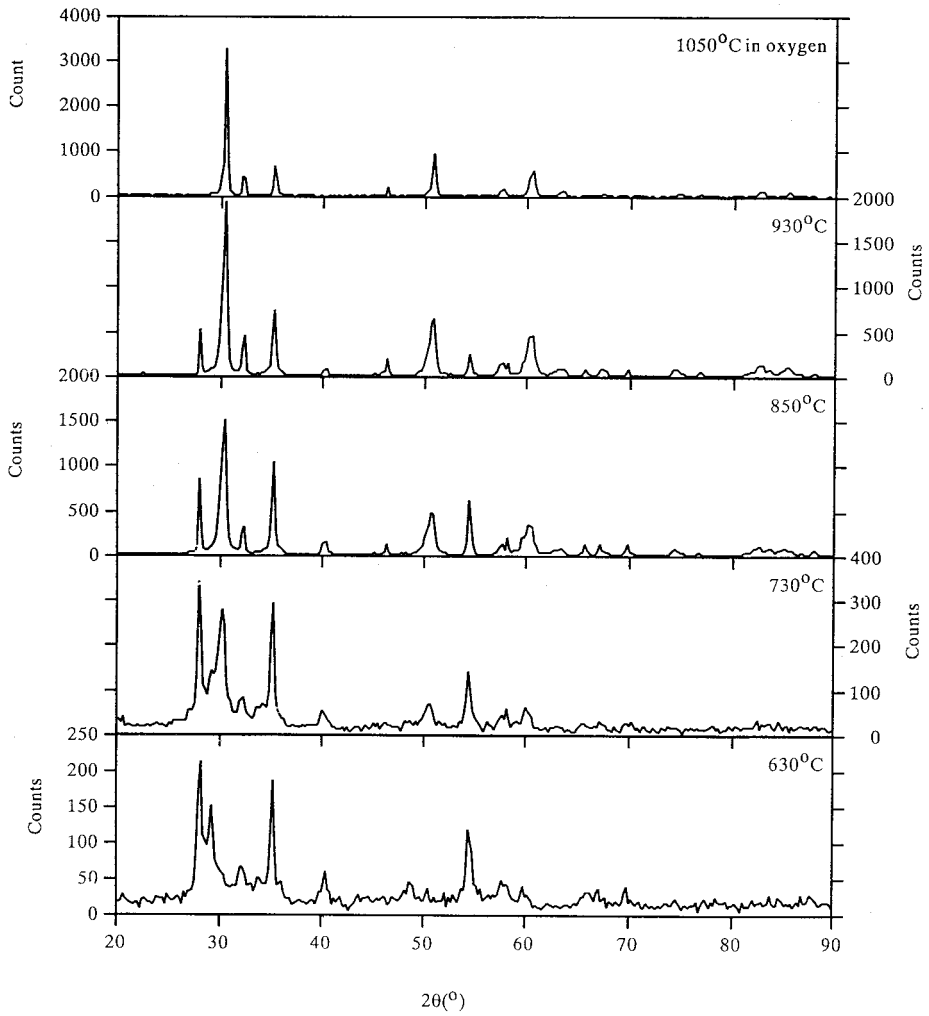


*Fig. 6.* Effect of heat treatment on YSRO films deposited at 400C by EACVD on CGO electrolye substrates. The YSRO films were crystallised by annealing at 800C.

to provide a useful measure of the overall cathodic kinetics for this situation. It is important to realise that this type of behavior is indicative of low oxygen diffusivities in the cathode grains. Tuller et al. [10] have indicated that undoped pyrochlores such as $Y_2Ti_2O_7$ have low ionic conductivities due to their highly ordered structure and in fact the ionic conduction is probably due to the presence of impurities. As the ionic radii of $Ti^{4+}$ and $Ru^{4+}$ are comparable, then a similar situation probably prevails for $Y_2Ru_2O_7$.

The doped material (YSRO) has similar microstructural features, and so it is reasonable to propose that the significant decrease in resistivity, $4200 \Rightarrow 154\,\Omega cm^2$ can be attributed to oxygen ion conductivity within the YSRO particles, that is the cathode material is a mixed conductor.

A model proposed by Adler et al. [22] for porous mixed conducting oxide cathodes provides a framework for examining the electrode resistivities measured in the present investigation. This model suggests that the electrode response of porous mixed conducting oxide electrodes is dominated by solid state diffusion and oxygen surface exchange. According to this model the effective ''chemical'' resistance is given by:

$$R_{\text{chem}} = \frac{RT}{2F^2}\sqrt{\frac{\tau}{(1-\varepsilon)aD_vC_vr_0}} \qquad (1)$$

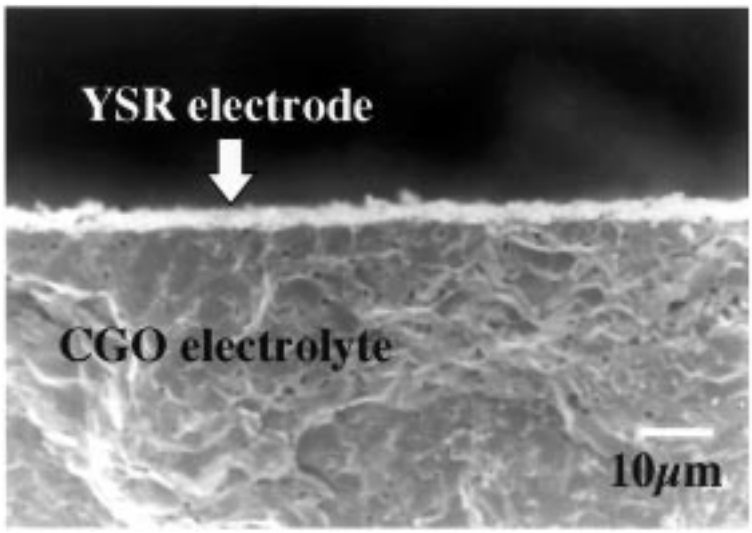


*Fig. 7.* SEM micrograph of fractured surface of YSRO film cathode deposited by EACVD.

where the microstructural parameters are represented by $\tau$ (tortuosity), $\varepsilon$ (fractional porosity), and a (internal surface area/unit volume). For the purpose of the present analysis these microstructural parameters are assumed constant for the thick (15 $\mu$m) electrode coatings to produce a value for $M$ $[\tau/(1-\varepsilon).a]$ equal to $6.1 \times 10^{-4}$ when $\tau = 1.5$, $\varepsilon = 0.3$, $a = 3500$. The product $C_v D_v$ can be replaced by $D^* C_o$ where $D^*$ is the oxygen self diffusion coefficient, and $C_o$ is the no. of moles of oxygen ions/unit volume. Finally $r_0$ is equal to $kC_o$ where $k$ is the oxygen surface exchange coefficient. Values of $D^*$ and $k$ are not available for $(Y_{0.8}Sr_{0.2})_2Ru_2O_7$ (YSRO) compositions and so it was decided to assume that the $k$ value for these compositions at 627C(900K) was comparable to the value measured [23] for $La_{0.6}Sr_{0.2}Co_{0.2}Fe_{0.8}O_{3-x}$, i.e., $5 \times 10^{-7}$ cm. s$^{-1}$. From Fig. 8b the total electrode resistivity for YSRO is approximately 154 $\Omega$cm$^2$. Substitution of this value in expression (1) requires the oxygen ion self diffusion coefficient to have a value around $1 \times 10^{-12}$ cm$^2$ s$^{-1}$ (Table 1) which would correspond to an ionic conductivity value around $10^{-7}$ Scm$^{-1}$. Ionic conductivity values of this magnitude are indicated by extrapolation to 900K of the results of Tuller et al. [10] for $Sm_{0.9}Sr_{0.1}Ti_2O_7$, which suggests that the present interpretation of the data is reasonable.

*3.3.2. $(Y_{1-x}Sr_x)_2Ru_2O_7$ cathode films (3 μm) prepared by EACVD.* A cathode film having the $(Y_{0.8}Sr_{0.2})_2Ru_2O_7$ composition had a resistivity of 114 $\Omega$cm$^2$ which may be explained by invoking slightly different microstructural parameters $(\varepsilon = 0.1, a = 5000)$ compared to the thick $(Y_{0.8}Sr_{0.2})_2Ru_2O_7$ samples (Table 1). The reduced porosity and slightly higher internal surface area (corresponding to smaller grain size) is supported by the SEM examination of a typical fracture surface of a $(Y,Sr)_2Ru_2O_7$ thick film electrode (Fig. 7) which depicts a relatively dense film incorporating submicron grains. However the lowest electrode

*Table 1.* Relationship between transport data and electrode resistivities

| Composition | $M$ cm | T C | $D$ cm$^2$ s$^{-1}$ | $k$ cm. s$^{-1}$ | $R_{chem}$ $\Omega$cm$^2$ |
|---|---|---|---|---|---|
| $(Y_{0.8}Sr_{0.2})_2Ru_2O_7$ (15 $\mu$m) | $*6 \times 10^{-4}$ | 627 | $1.0 \times 10^{-12}$ | $5.0 \times 10^{-7}$ | 155 |
| $(Y_{0.8}Sr_{0.2})_2Ru_2O_7$ (3 $\mu$m) | $**3.3 \times 10^{-4}$ | 627 | $1.0 \times 10^{-12}$ | $5.0 \times 10^{-7}$ | 115 |
| $(Y_{0.8}Sr_{0.2})_2Ru_2O7$ (3 $\mu$m) | $**3.3 \times 10^{-4}$ | 627 | $1.0 \times 10^{-12}$ | $5.0 \times 10^{-7}$ | 47 |
| $La_{0.6}Sr_{0.4}Co_{0.2}Fe_{0.8}O_3$ | $*6 \times 10^{-4}$ | 627 | $5.2 \times 10^{-10}$ | $5.5 \times 10^{-7}$ | 6.5 |
| $(Gd_{0.95}Sr_{0.05})_2Ru_2O_7$ | $*6 \times 10^{-4}$ | 627 | $6.0 \times 10^{-9}$ | $5.0 \times 10^{-7}$ | 2.0 |

$M = \tau/(1-\varepsilon;)a$ $*(\tau = 1.5, \varepsilon = 0.3, a = 3500\,\text{cm}^{-1})$ $**(\tau = 1.5, \varepsilon = 0.1, a = 5000\,\text{cm}^{-1})$.

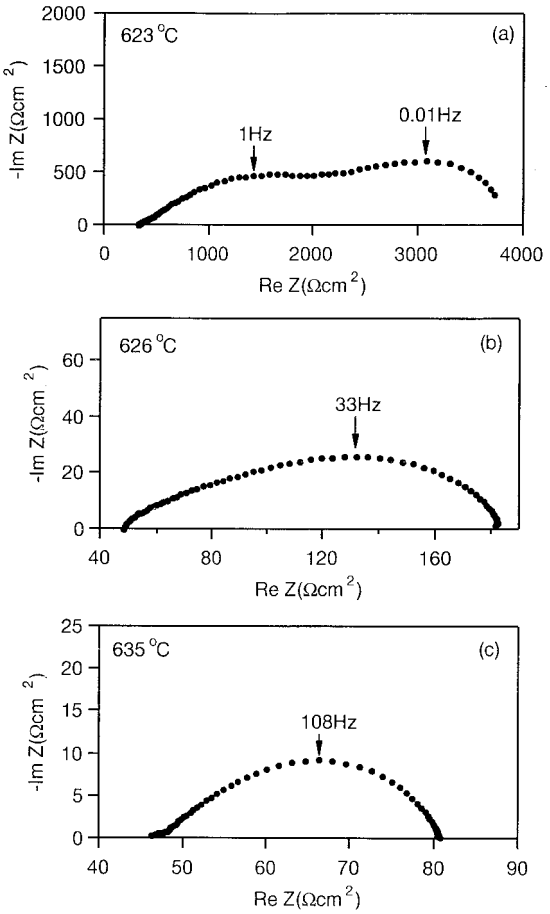


*Fig. 8.* (a) Complex impedance of undoped thick (15 $\mu$m) $Y_2Ru_2O_7$ cathode on CGO electrolyte. (b) Complex impedance of $(Y_{0.8}Sr_{0.2})_2Ru_2O_7$ thick (15 $\mu$m) cathode on CGO electrolyte. (c) Complex impedance response of $(Y_{0.95}Sr_{0.05})_2Ru_2O_{7-x}$ film cathode fabricated by EACVD method on CGO electrolyte.

resistivity at 635C (45 $\Omega cm^2$) was obtained with 5% SrO doping levels see Fig. 8(c). Assuming all the microstructural parameters remain the same then an oxygen self diffusion coefficient of $6 \times 10^{-12}\,cm^2\,s^{-1}$ (Table 1) can account for the observed lower electrode resistivity. It is interesting to note that Tuller et al. [10] obtained a maximum in the oxygen ion conductivity of $(Gd_{1-x}Ca_x)_2Ti_2O_7$ compositions for values of $x$ around 0.1. Moreover the maxima in ionic conductivity was associated with lower activation energies ( $\sim$ 0.6 ev). The activation energies of the electrode resistivities examined in the present investigation are somewhat higher, typically around 1 eV (Fig. 9). Again this would be expected from the data of Tuller et al. [10] who examined ionic

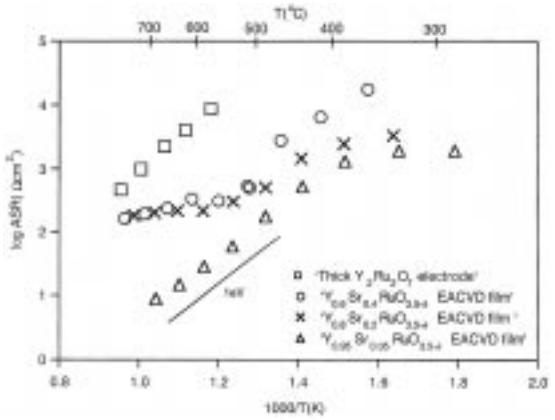


*Fig. 9.* Electrode resistivity for various compositions of strontium-doped yttrium ruthenate as a function of reciprocal temperature. Original impedance data at various temperatures are available in [23].

conduction in the $Sm_2Ti_2O_7$ doped with SrO, CaO, and MgO. The highest conductivity and lowest activation energy were associated with the CaO dopant as the size of this ion is a better match to the host cation Sm than the other dopants which are either too large or too small. As $Y^{3+}$ is smaller than $Sm^{3+}$ than the dopant-host mismatch is even greater for SrO which is in accordance with the relatively high activation energies ( $\sim$ 1 eV) recorded for the SrO-doped $Y_2Ru_2O_7$ electrode compositions. Finally it should be noted that further details of the impedance measurements as a function of temperature are available [24].

The proposed interpretation of the impedance data in terms of oxygen self diffusion and surface exchange coefficients has the merit of being internally self-consistent, and in accordance with the ionic conductivity trends for rare earth titanate pyrochlore compositions established by Tuller and co-workers [8]. However the assumptions implicit in this interpretation certainly require further examination. For example, although the rutile phases, $TiO_2$ and $RuO_2$, have similar lattice parameters only a small mutual solubility exists [25] due to differences in the $3d(Ti^{4+}) - 2p(O^{2-})$ and $4d(Ru^{4+}) - 2p(O^{2-})$ orbital interactions [26], and so care has to be taken in drawing too many parallels between $Gd_2Ti_2O_7$ and $Y_2Ru_2O_7$. In this context it is interesting to note that Tuller and Spears [12] interpret their data for $Gd_2(Ti_{1-x}Ru_x)_2O_7$ in terms of almost complete reduction of $Ru^{4+}$ to $Ru^{3+}$ at moderate temperatures (750C). However this is most unlikely as the 4d $Ru^{4+}$

ion is relatively stable in oxides until the oxygen partial pressure is sufficiently low to cause reduction to metallic Ru, and there is no evidence [27] for the formation of an intermediate sesquioxide, $Ru_2O_3$. Bourchard and Gillson's claim [28] that $Y_2Ru_2O_7$ is essentially stoichiometric is supported by the work of Peacock [29] on the stoichiometry of $RuO_2$ which only indicates a narrow range of homogeneity, $RuO_{1.98} - RuO_{2.015}$ in the temperature range 500–600C. More recently Linquette-Mailley et al. [18] suggest that the the stoichiometric range for $Bi_2Ru_2O_{7.3}$ is also relatively small. It thus appears that in $Y_2Ru_2O_7$ most of the ruthenium is present as $Ru^{4+}$, and so the introduction of $Sr^{2+}$ $(Sr'_Y)$ will probably be compensated by the formation of oxygen ion vacancies $(V_o^{\cdot\cdot})$, although a small concentration of $Ru^{5+}$ $(Ru^{\cdot}_{Ru})$ may also be produced. The formation of anion vacancies is, of course, consistent with the interpretation proposed earlier to explain the impedance data.

The data of Tuller and Spears [11,12] do suggest that it should be possible to obtain oxygen diffusion coefficients exhibiting values of at least $6 \times 10^{-9}\,cm^2\,s^{-1}$ (i.e., $\sigma_i \sim 6 \times 10^{-4}\,Scm^{-1}$) at 627C for compositions in the CaO doped $Gd_2Ru_2O_7$ series. Such values would lead to cathode resistivities at least 3 times lower than those associated with LSCF (Table 1), which support the case for further investigations in this area.

## Conclusions

$Bi_2Ru_2O_{7.3}$ and $Pb_2Ru_2O_{6.5}$ powders react with $Ce_{0.9}Gd_{0.1}O_{1.95}$ (CGO) electrolyte powders at 900C and cannot be considered as appropriate cathode materials for CGO. In contrast $Y_2Ru_2O_7$ appeared to be stable in contact with CGO and was examined as a candidate cathode material. Impedance measurements indicated that $Y_2Ru_2O_7$ exhibited very high ASR values ( $\sim 4000\,\Omega cm^2$) at 627C. Doping with 5 mole% SrO reduced the ASR to $47\,\Omega cm^2$ at 627C. The behavior of the $Y_2Ru_2O_7$ cathodes was interpreted in terms of oxygen ion diffusion and surface exchange coefficients which suggested that the behavior of ruthenate cathodes could be further improved so that they should have superior performance to $La_{0.6}Sr_{0.4}Co_{0.2}Fe_{0.8}O_3$ electrodes at intermediate temperatures.

## Acknowledgments

The authors wish to acknowledge financial support from the Korean government, and Johnson Matthey Co. who also supplied the ruthenium nitrosyl nitrate.

## References

1. M. Watanabe, H. Uchida, M. Shibata, N. Mochizuki, and K. Amikura, *J. Electrochem. Soc*., **141**, 342 (1994).
2. M. Sahibzada, S.J. Benson, R.A. Rudkin, and J.A. Kilner, in *Proc. 11th Int. Conf. on Solid State Ionics* (Hawai, Nov. 1997). To be published in *Solid State Ionics* (1998).
3. H. Sasaki, M. Susuki, S. Otoshi, A. Kajimura, and M. Ippommatsu, *J. Electrochem. Soc*., **139**, L12 (1992).
4. M. Hrovat, J. Holc, and D. Kolar, *Solid State Ionics*, **68**, 99 (1994).
5. M.A. Subramanian, G. Aravamudan, and G.V. Subba Rao, *Prog. Solid State Chem*., **15**, 55 (1983).
6. H.S. Horowitz, J.M. Longo, H.H. Horowitz, and J.T. Lewandowski, *Am. Chem. Soc. Symp. Series*, **279**, 143 (1985).
7. R.G. Egdell, J.B. Goodenough, A. Hamnett, and C.C. Naish, *J. Chem. Soc., Faraday Trans. 1*, **79**, 893 (1983).
8. N.M. Markovic and P.N. Ross jr., *J. Electrochem. Soc*., **141**, 2590 (1994).
9. J.D. Faktor, J.A. Kilner, and B.C.H. Steele, *Proc. 2nd. European Conf. on Solid State Chemistry* eds R. Metselaar, H.J.M. Heijligers and J. Schoonman (Elsevier, 1982), p. 207.
10. H.L. Tuller, S. Kramer, and M.A. Spears, in *Proc 14th Riso Symp. on Materials Science* eds F.W. Poulsen et al. (Riso National Lab., Denmark, 1993), p. 151.
11. M.A. Spears and H.L. Tuller, in *Proc. 2nd Intl. Symp. on Ionic and Mixed Conducting Ceramics*, eds T.A. Ramanarayanan, W.L. Worrell, and H.L. Tuller, *ECS Proc. Vol. 94-12* (Electrochemical Society, New Jersey, USA, 1994), p. 94.
12. H.L. Tuller and M. Spears, in *Proc. 1st European SOFC Forum*, ed. U. Bossel, (ISBN 3-922-14-X, Switzerland, 1994), p. 435.
13. M. Pechini, US. Patent 3,330,697 (11 July, 1967).
14. L.A. Chick, L.R. Pederson, G.D. Maupin, J.L. Bates, L.E. Thomas, and G.J. Exarhos, *Materials Lett*., **10**, 6 (1990).
15. P.A. Lane, *Investigations of the Vapor Phase Growth of Oxide Films from Metal Alkoxides* (Ph.D Thesis, University of London, October, 1988).
16. K.-L. Choy, W. Bai, and B.C.H. Steele, in SOFC-V, *Proc. Vol 97-40*, eds U. Stimming et al. (Electrochem. Soc., New Jersey, USA, 1997), p. 1177.
17. A.A. van Zomeren, E.M. Kelder, J.C.M. Marijnissen, and J. Schoonman, *J. Aerosol Sci*., **25**, 1229.
18. S. Linquette-Mailley, A. Caneiro, E. Djurado, G. Mairesse, and J. Fouletier, *Solid State Ionics*, **107**, 191 (1998).
19. Y. Senzaki, M.J. Hampden-Smith, T.V. Kodas, and J.W. Hussler, *J. Am. Ceram. Soc*., **78**, 2977 (1995).
20. F.H. van Heuveln and H.J.M. Bouwmeester, *J. Electrochem. Soc*., **144**, 134 (1997).
21. B.C.H. Steele, *Solid State Ionics*, **94**, 239 (1997).
22. S.B. Adler, J.A. Lane, and B.C.H. Steele, *J. Electrochem. Soc*., **143**, 3554 (1996).

23. S.J. Benson, R.J. Chater, and J.A. Kilner, in *Proc. 3rd Intl. Symp. on Ionic and Mixed Conducting Ceramics*, eds T.A. Ramanarayanan, W.L. Worrell, and H.L. Tuller, *ECS Proc. Vol. 97-24* (Electrochemical Society, New Jersey, USA, 1997), p. 596.
24. J.-M. Bae, *Properties of selected oxide cathodes for solid oxide fuel cell* (Ph.D Thesis, University of London, May, 1996).
25. P. Triggs, *Helvetica Physica Acta*, **58**, 657 (1985).
26. P.A. Cox, *Transition Metal Oxides* (Oxford, 1992).
27. F.P.F. van Berkel, *Ruthenates: Phase Relations, Structural and Catalytic Properties*, (Ph.D. Thesis, University of Leiden, Netherlands, December, 1988).
28. R.J. Bourchard and J.L. Gillson, *Mater. Res. Bull.*, **6**, 669 (1971).
29. H.M. Peacock, *Solid State Oxide Chemistry of Ruthenium* (Ph.D. Thesis, University of Aberdeen, November, 1988).